LAWRENCE
LIVERMORE
NATIONAL
LABORATORY

LLNL-JRNL-564814

Local Reflow of AuSn Solder: Relating Strength to Microstructure

I. V. Golosker, J. N. Florando

July 17, 2012

Welding Journal

Disclaimer

This document was prepared as an account of work sponsored by an agency of the United States government. Neither the United States government nor Lawrence Livermore National Security, LLC, nor any of their employees makes any warranty, expressed or implied, or assumes any legal liability or responsibility for the accuracy, completeness, or usefulness of any information, apparatus, product, or process disclosed, or represents that its use would not infringe privately owned rights. Reference herein to any specific commercial product, process, or service by trade name, trademark, manufacturer, or otherwise does not necessarily constitute or imply its endorsement, recommendation, or favoring by the United States government or Lawrence Livermore National Security, LLC. The views and opinions of authors expressed herein do not necessarily state or reflect those of the United States government or Lawrence Livermore National Security, LLC, and shall not be used for advertising or product endorsement purposes.

Local Reflow of AuSn Solder: Relating Strength to Microstructure

Ilya Golosker, Mechanical Engineer, Lawrence Livermore National Laboratory
Jeff Florando, Materials Scientist, Lawrence Livermore National Laboratory

Local heating of AuSn solder creates reliable bonds. However, small changes in the heat schedule result in significant changes to bond strength and microstructure.

Introduction

Modern microchips, sensors, and micro-electromechanical systems (MEMS) have precipitated the development of soldering processes that avoid the use of corrosive flux. Various solutions have been developed for this challenge, and a fluxless soldering process must optimize bond strength while minimizing temperature effects during reflow. Furthermore, performing solder bonds in atmospheric conditions is desirable because it alleviates complications inherent to processing in an inert gas environment. Systems with sensitive polymers must remain below certain temperatures and time thresholds while the hard solder reaches extreme reflow temperatures. Understanding how heating recipes affect the strength, microstructure and composition of a fluxless solder is valuable in optimizing production processes.

The use of hard solder has several advantages in microelectronics applications, including high thermal stability (Ref. 1) and good thermal conductivity for heat dissipation (Ref. 2). The price for these advantages is a high reflow temperature that may damage polymers and other temperature sensitive components. Localized heating can be optimized to create high temperature gradients that limit the flow of the solder to the specified joint (Ref. 3) and control the temperature distribution. A maximized temperature gradient was found to best satisfy these parameters. Overall, the decision to utilize hard solders must take into account their high strength and good fatigue resistance (Ref. 6), in exchange for the transmission of stresses not seen in soft solders.

Fluxless 78Au22Sn solder bonds were successfully created using a thermode in atmosphere. The samples were shear tested to determine the bond strength. Electron microscopy with energy dispersive X-ray spectroscopy (EDAX) was performed to inspect microstructure and the formation of intermetallic phases, and nanoindentation was used to determine material properties. Small changes in thermode hold time and temperature were found to influence the microstructure and strength of the solder.

Materials and Methods

Preformed pieces of 0.038 mm thick, homogenous 78Au22Sn (wt. %) fluxless solder (AIM, Cranston, RI) were used to join a Cu stripline and alumina chip. The Cu stripline, used to carry current to the desired component, was metalized for soldering with an Electroless Nickel Immersion Gold (ENIG) finish of 4µm of Ni and 0.5 µm of gold. The chip layer consists of 0.5 mm thick alumina with deposited layers of Ti, Au, Ni, and Au. The chip and stripline were placed on a working surface of either machined copper or fiberglass-reinforced phenolic resin substrate during soldering. A schematic of the metallization is presented in Figure 1.

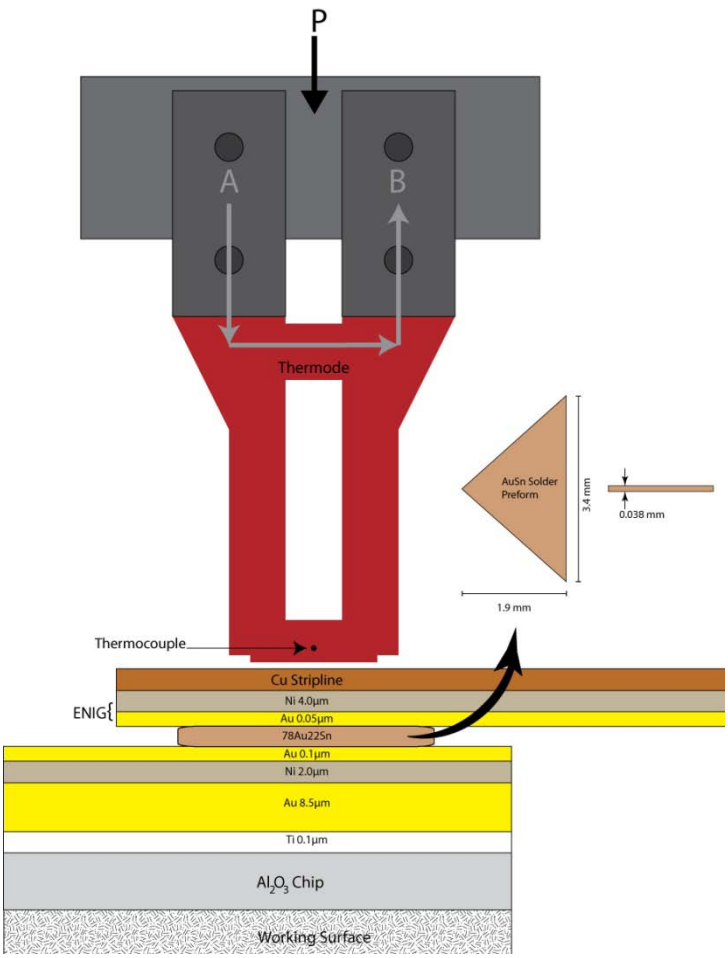

Figure 1: A schematic of the metallization layers in a soldering sample with the thermode used to reflow the solder. A thermode is heated by passing current from point A to B, and a thermocouple is attached to the bottom of the thermode for feedback control to the power supply. The thermode assembly lowers with a force P to make contact with the chip and solder assembly.

Soldering

Reflow of the solder was achieved using a thermode to send a thermal pulse into the chip assembly, as seen in Figure 1. A Miyachi-Unitek ThinLine 87A thermode head with a Uniflow 2 power supply allows for control of the soldering recipe and load on the thermode. The thermode was fabricated from molybdenum and customized to conform to the shape of the triangular solder preforms, also seen in Figure 1. An electric current was passed from point A to B in Figure 1 for Joule heating of the thermode, resulting in a temperature gradient going downward to the stripline. A K-type thermocouple was attached near the bottom of the thermode for feedback control to the power supply. As per the

schematic in Figure 1, the alumina chip was placed on the bottom with the Cu stripline on top in contact with the thermode. Hardware was machined to align the sample underneath the thermode. Heating recipes for all samples had a rise time of 1 sec, while hold times and thermode temperatures were varied.

Finite element simulations with a FlexPDE partial differential equation solver (Ver. 6.15, www.pdesolutions.com) were used to investigate the processing surface on which the samples were soldered. The simulations were modeled in a mesh with 29,160 nodes in cylindrical coordinates, solving the heat equation in discrete time steps. The meshed domains can be seen in Figure 2a. The effects of a Cu heat-sink surface (k=386 W/m-K, Ref. 8) and insulating Bakelite phenolic resin surface (k=0.52 W/m-K, Ref. 9) were compared by inspecting time profiles of heating recipes. While a Cu heat sink layer lowered the temperature of the front of the package, a corresponding drop was found in the solder temperature, necessitating increased temperatures and hold times to achieve reflow. As seen below in Figure 3b, the solder temperature profile corresponding to a 600 °C peak temperature at the thermode is 50-100 °C lower with a Cu heat-sink. In order to reduce the temperature of the front of the package while achieving reflow of the solder, a Bakelite bottom layer was used for all tests. The model was used to estimate a heating profile to produce peak temperatures up to 200 °C above the melting point of the solder to achieve proper reflow.

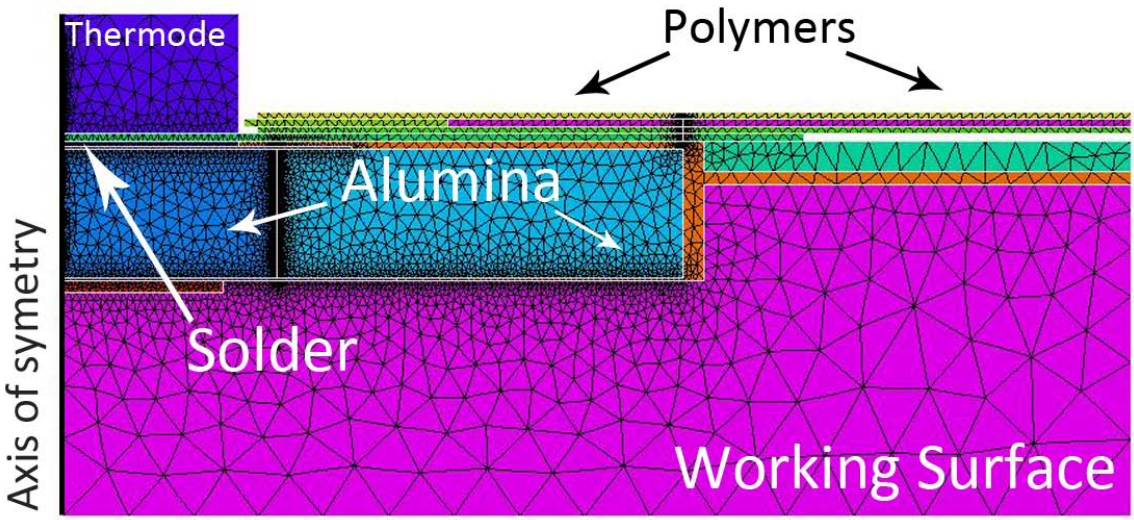

Figure 2a: Diagram of the meshed regions of the Flex PDE finite element simulation of the soldering. The working surface domain was varied from a Cu heat sink to an insulating phenolic material to determine the optimal surface for solder reflow.

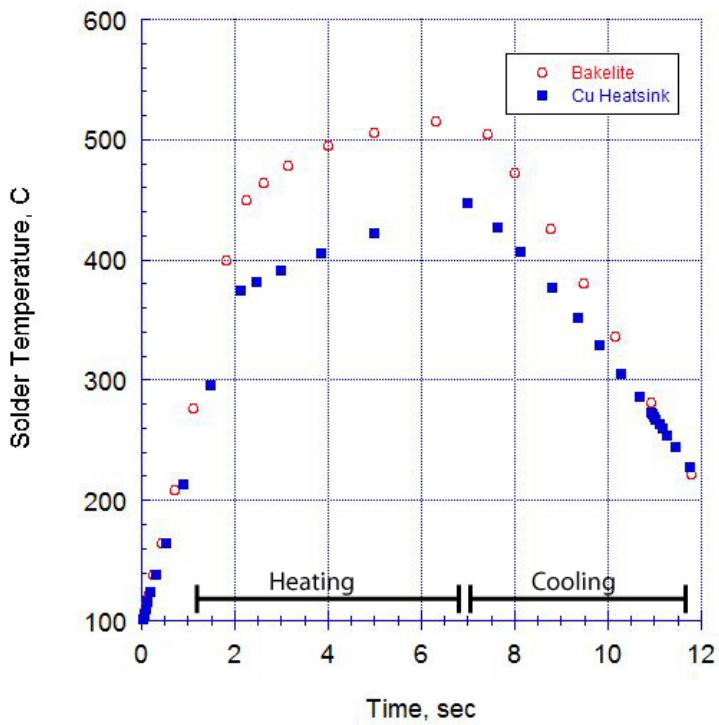

Figure 2b: Solder temperature versus time plot for a finite element simulation of a 600 °C heating recipe. A heating recipe driving the temperature of the thermode simulates the heating and cooling cycles of the solder.

Shear Testing

Solder bond strength was tested using an MTS 0.5 kN electro-mechanical load frame and MTS TestWorks software acquiring data at 50 Hz. Fixtures for the tensile test machine supported the sample and constrained motion to minimize bending and ensure a shear stress state. The Cu stripline was bonded to an Al bar with 3M DP420 epoxy. The bar was attached to the lower fixture using a clamp, as seen in Figure 3. The substrate was supported from the bottom by an Al cutout and bending was minimized with a supporting bracket near the top of the sample. The displacement rate of the test fixture was controlled to 0.05 in/min to represent quasi-static loading. After failure, the wetted area of the solder was able to be observed and its area was calculated using image analysis software. The quotient of the maximum machine load and wetted area was used to calculate shear stress.

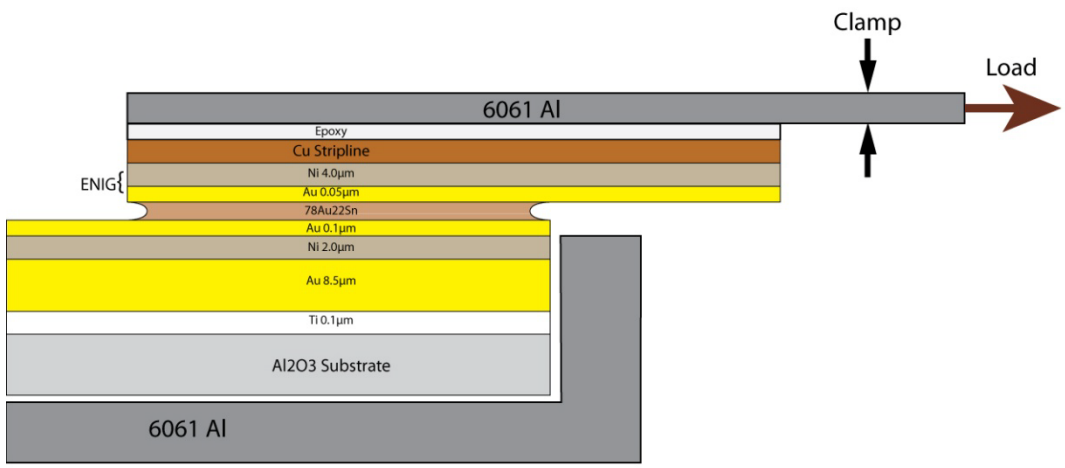

Figure 3: A schematic of the mechanical testing of a solder sample. An Al block is used to support the substrate and is attached to the stripline layer. The setup minimizes bending and produces a shear force at the solder layer.

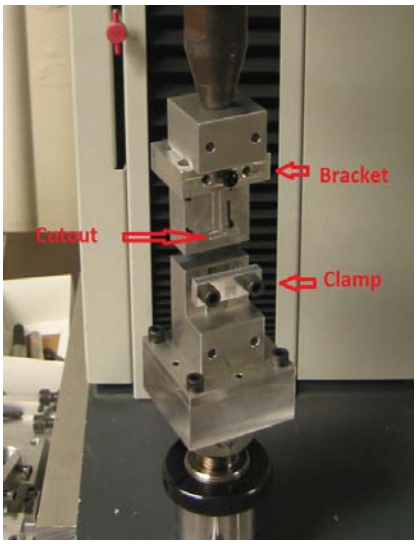

Figure 4: Fixtures for mechanical testing of a solder sample in a tensile testing machine. The bracket and clamp in the image are used to counteract bending of the sample.

Characterization

Intermetallic compounds were identified using the EDAX system (www.edax.com) for energy dispersive X-ray spectroscopy. The system uses a 1.3 µm Parylene window to detect the response to an X-ray excitation. Calibration was performed with a manganese target and a Fe^{55} radioisotope as an X-ray source to detect MnKα and MnKβ excitation signals.

Nanoindentation

Nanoindentation measurements were made on solder cross sections after shear testing. The samples were cross sectioned across the reflow zone and mounted in 615 Light Blue epoxy (Dexter Corp). Diamond powder was used to first polish the alumina substrate and not over-polish the solder joint. Then 1 µm colloidal alumina was used to finish the polish to minimize scratching and smearing of the soft metallization layers.

Measurements of hardness and modulus of elasticity were achieved with an Agilent Nanoindenter G200 with an XP head. A diamond Berkovich indenter was used to a depth of 2000 nm. Modulus and hardness values were obtained as a function of indentation depth, and data deeper than 1µm was considered to

minimize the surface effects at small depths. The strain rate target of the indentation was set to 0.05/s for all tests. Multiple indentations were made along each solder cross section, allowing for statistical analysis of the data. A fused silica standard with known modulus and hardness was used for calibration and determination of the indenter tip area function.

Results and Discussion

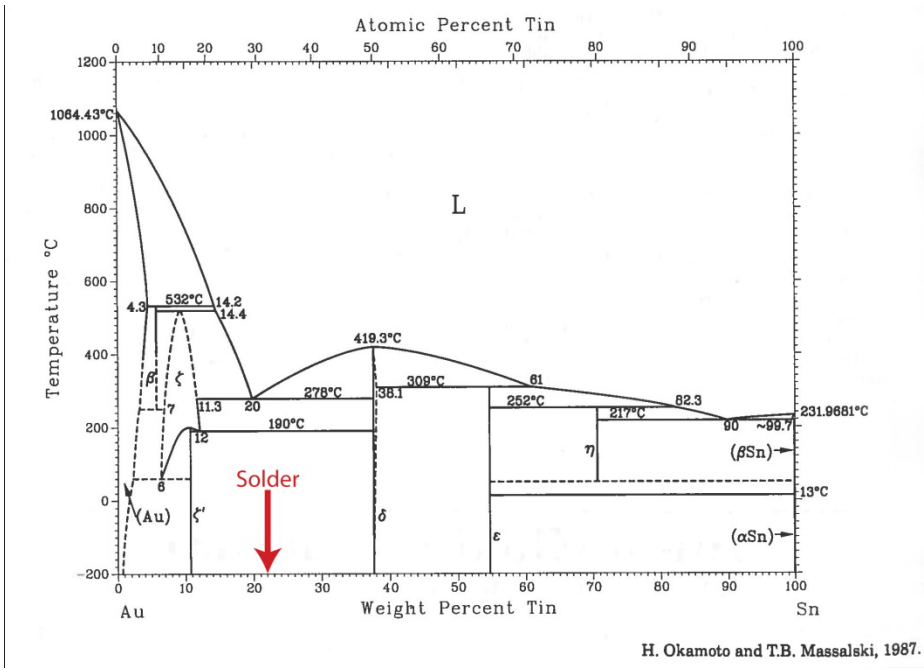

Figure 5: Phase diagram for Au-Sn solder (Ref. 7). The arrow notes the 78/22 wt. % composition of the AuSn solder.

The first sample was soldered with a 575°C thermode temperature held for 1.5 sec. Thermode temperatures well above the 282 °C melting point of the alloy are necessary for adequate heat to transfer through the metallization layers in the short hold time. The sample was mechanically tested and the bond failed in the solder layer at a shear stress of 13.8 MPa. A lamellar eutectic structure of alternating phases of eutectic Au_5Sn (ζ') and AuSn (δ) phases formed, which is expected based on the phase diagram, seen in Figure 6. The solder and metallization layers can be seen in Figure 6a. The high magnification SEM micrograph, Figure 6b, shows δ phase intermetallics interspersed throughout the

solder thickness, which is consistent with the Sn-rich hypereutectic 78/22 wt. % AuSn composition. Rapid cooling of the sample when the thermode lifted from the chip assembly resulted in a fine eutectic lamellar structure with a spacing of 0.25 µm. Nanoindentation measurements showed a modulus of 73.1±6.0 GPa and hardness of 2.56 ± 0.40 GPa. The solder preforms and reflow area can be seen in Figures 7a and 7b, which are visually similar to the other samples.

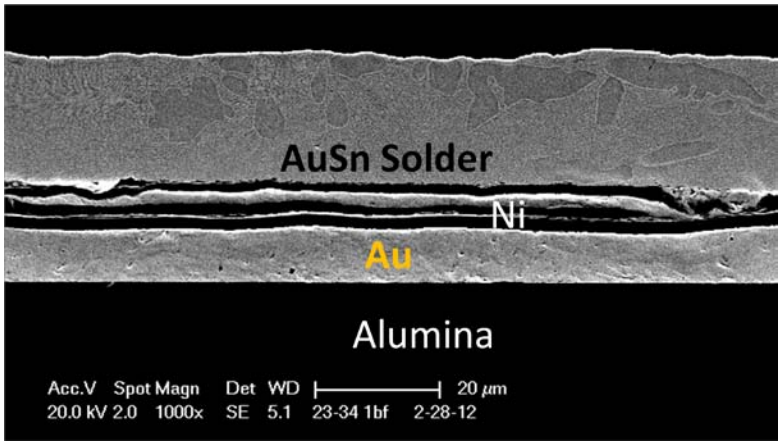

a)

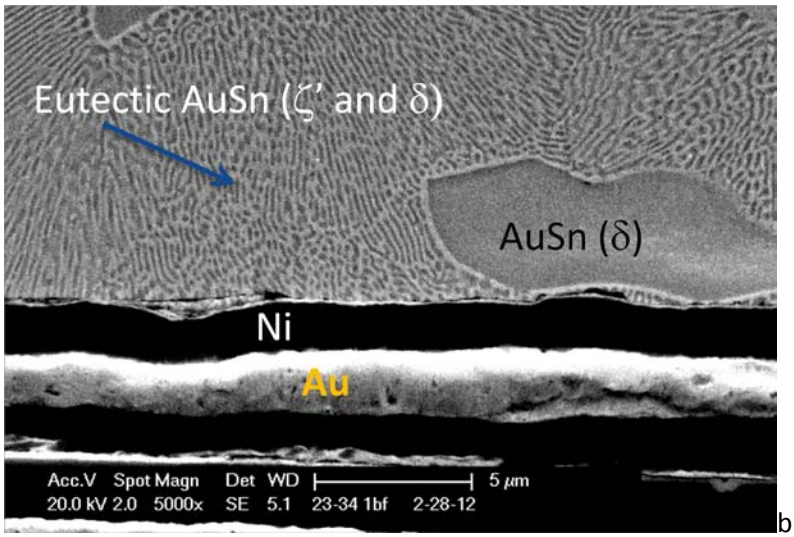

b)

Figure 6a: A low magnification scanning electron micrograph the solder, nickel, gold and alumina layers of the chip assembly heated to 575 °C and held for 1.5 seconds. Figure 6b: A high magnification image of the gold and nickel layer as well as the eutectic phases and δ phases formed in the solder.

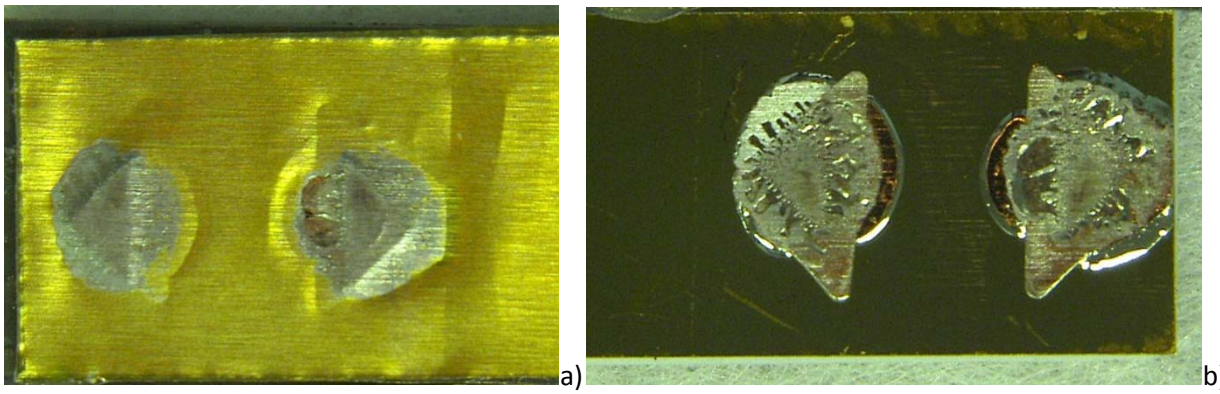

Figure 7a: Photograph of the failed solder bond on the ENIG layer of first sample. Figure 7b: The reflow area of the solder is clearly visible on the bottom half of the sample.

The second sample was heated to 575 °C and held for a longer time of 2 sec. Mechanical testing resulted in a shear stress of 20.0 MPa at failure. A low magnification SEM image can be seen in Figure 8a. Figure 8b shows similar micro structural features with a ζ' and δ phase eutectic with δ phase intermetallics in the solder. The δ primary solidification phase also emanates from the Au layer at the bottom 2-5 µm of the solder layer. A higher shear stress of 20 MPa measured from mechanical testing is an indication of a stronger bond. Nanoindentation testing resulted in a modulus measurement of 74.0 ± 3.0 GPa and hardness of 2.68 ± 0.1 GPa. While the mechanical properties were not statistically different from the sample heated for less time, the shear stress at failure was higher. The δ intermetallic phase and eutectic microstructure at the interface of the bottom Au and AuSn solder indicate increased dissolution of Au into the solder during reflow.

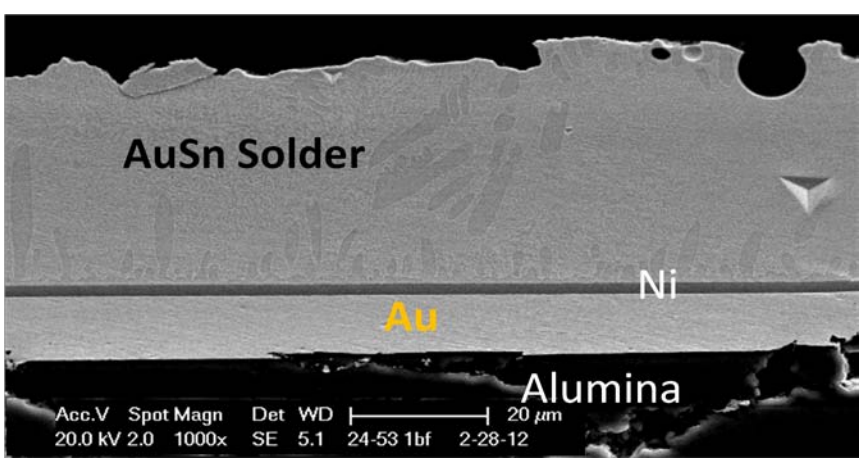

a)

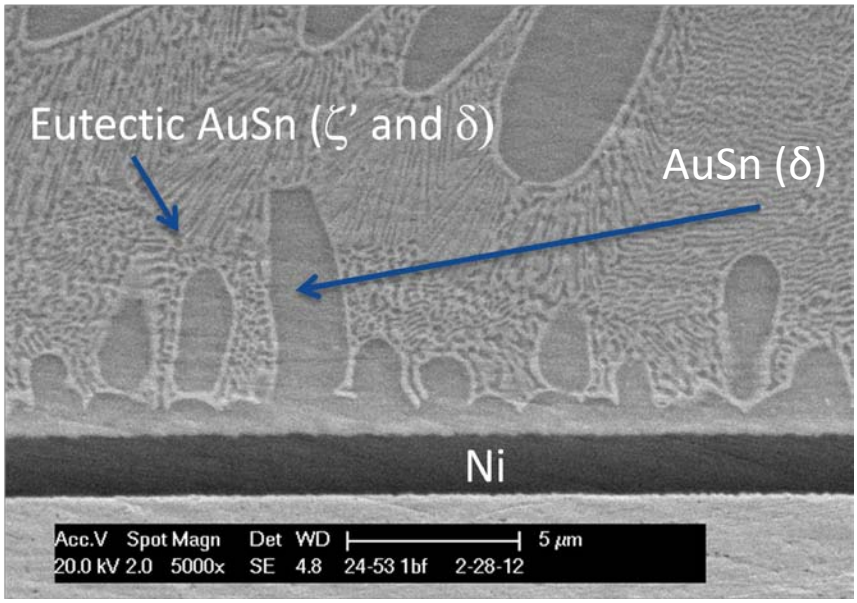

b)

Figure 8a: A scanning electron micrograph of the solder assembly cross-section heated to 575 °C and held for 2 seconds. The alumina chip and deposited gold and nickel layers underneath the solder are visible. Figure 8b: A high magnification micrograph showing the nickel layer and solder. The gold layer is not discernable, and gold-rich δ phase intermetallics emanate from the interface.

The third sample was heated to 600 °C and held for 4 seconds, providing the most severe heating cycle of the three tests. The highest shear strength of 24.9 MPa resulted from the sample breaking through the epoxy layer and tearing the Cu stripline while the solder stayed intact. The calculated shear strength is in good agreement with the manufacturer's documented room temperature overlap shear strength of 24.1 MPa (3500 psi) for epoxy bonded to aluminum that had not been etched (Ref. 10). The eutectic ζ' and δ lamellar structure was observed, but now $(AuNi)_3Sn_2$ intermetallics were also present in the solder based on EDAX analysis. Micrographs of the sample are shown in Figures 9a and 9b. Nanoindentation resulted in a modulus measurement of 83 ± 5 GPa and hardness of 2.69 ± 0.10 GPa. During heating the gold completely dissolved in the solder, and the higher temperature allowed for the nickel layer to react and form Ni rich intermetallics. The $(AuNi)_3Sn_2$ intermetallic compounds may be responsible for the significant increase in shear strength.

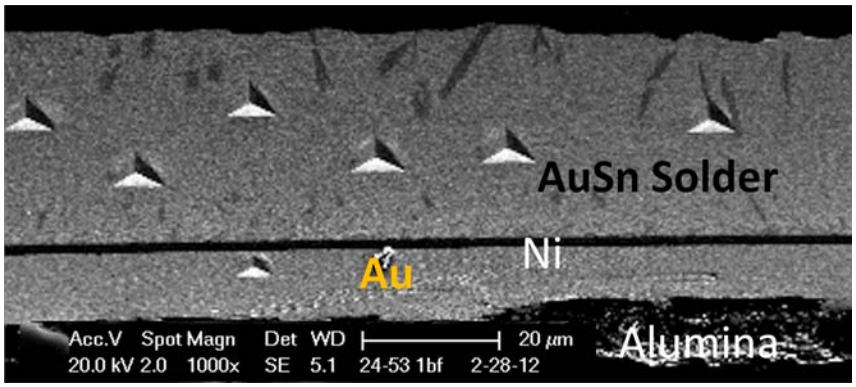

a)

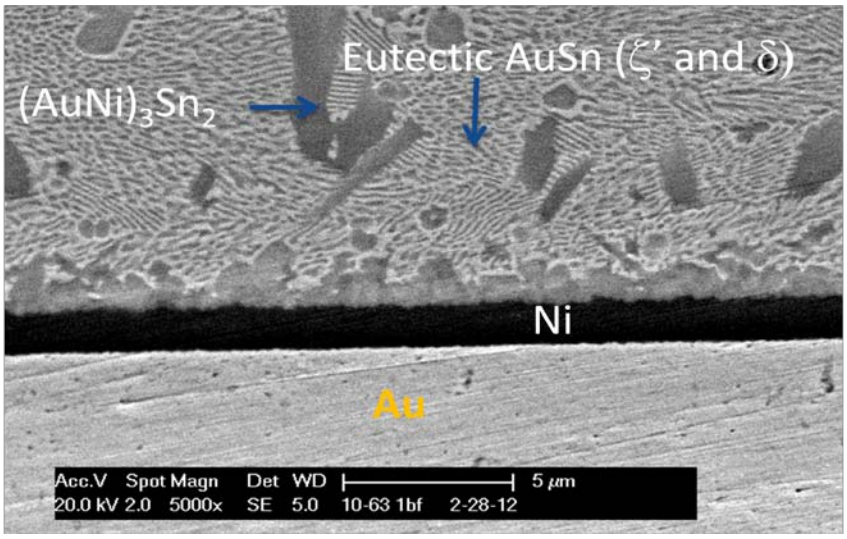

b)

Figure 9a: A scanning electron micrograph of the solder assembly cross-section heated to 600 for 4 seconds. Triangular indentation marks are visible from the Nanoindentation measurements. Figure 9b: A high magnification micrograph of the gold, nickel and solder layer. Nickel-rich intermetallic phases are visible, due to the gold layer completely dissolving in the solder.

Table 1 below summarizes the mechanical properties measured with nanoindentation as well as the shear stress at failure. The hardness did not differ between samples, but the modulus of the sample with the $(AuNi)_3Sn_2$ intermetallics is higher than the other samples. The modulus values for the first two samples are consistent with Chromik's results on the eutectic composition, as seen in Table 2. The finer lamellar structure (0.25 µm versus 10 µm in Chromik) is responsible for the comparably higher hardness values in all three samples. The stiffness of the $(AuNi)_3Sn_2$ phase in the third sample may be responsible for the higher modulus value. Similar intermetallics were found in other studies where the samples were annealed and thermally aged, but were found to decrease the toughness of the joint (Ref. 5).

Table 1: Summary of nanoindentation and shear testing results.

Sample	Thermode Temperature (°C)	Hold Time (Sec)	Modulus (GPa)	Hardness (GPa)	Shear Stress (MPa)
1	575	1.5	73.1 ± 6.0	2.56 ± 0.4	13.1
2	575	2	74 ± 3.0	2.68 ± 0.1	20.0
3	600	4	83 ± 5.0	2.69 ± 0.1	24.9*
*failure in epoxy layer					

Table 2: Summary of results from Chromik, et al. (Ref. 4).

Results from Chromik et al. (Ref. 4)		
Phase	Modulus (GPa)	Hardness (GPa)
Eutectic	76 ± 5	1.3 ± 0.2
Au_5Sn (ζ')	74 ± 5	2.5 ± 0.2
AuSn (δ)	87 ± 9	1.4 ± 0.1
(Eutectic spacing ~10 µm)		

Conclusion

Fluxless AuSn solder was successfully reflowed in atmosphere using a thermode. The Au layers contacting the solder preform prevented the formation of oxides which would hinder the reflow process. The ability to join components without an inert gas environment allows for greater freedom in designing experiments and production processes with predictable localized reflow without unnecessarily heating the entire assembly in an oven.

Changes in hold time from 1.5 to 4 seconds and thermode temperatures ranging from 575 to 600 °C were found to nearly double the strength of the solder bond. The growth of δ phase intermetallics can be correlated to a 50% increase in bond strength with a 0.5 second longer hold time, and Ni rich intermetallics result in bond strength of at least 24.8 MPa. Local heating to achieve reflow of hard

solders has the potential to control the reflow area and temperature distribution, resulting in strong solder bonds.

Acknowledgements

The authors would like to thank Barry Olsen for his help in soldering, Mary Leblanc and Victor Hepa for their work in bond testing. Thank you to John W. Elmer for helpful feedback and commentary throughout the writing of the article. We would also like to thank Chris Walton for the development of the FEA model.

References

1. Aasmundtveit, K.E.; Wang, K.; Hoivik, N.; Graff, J.M.; Elfving, A.; , "Au–Sn SLID bonding: Fluxless bonding with high temperature stability to above 350 °c," *Microelectronics and Packaging Conference, 2009. EMPC 2009. European* , vol., no., pp.1-6, 15-18 June 2009
2. Yoon, J.W.; Chun, H.S.; Koo, J.M.; Jung, S.B.;," Au–Sn flip-chip solder bump for microelectronic and optoelectronic applications," *Microsystem Technologies*, vol. 13., no. 11, pp.1463-1469, June 2007, Doi: 10.1007/s00542-006-0330-9
3. Humpston, G.; Jacobson, D.M; Principles of Soldering and Brazing. ASM International, 1993. ISBN: 0-87170-462-5
4. R.R. Chromik, D.-N. Wang, A. Shugar, L. Limata, M.R. Notis and R.P. Vinci, "Mechanical properties of intermetallic compounds in the Au-Sn system.", *Journal of Materials Research* 20, 2161 (2005).
5. Zribi, A.; Chromik, R.R.; Presthus, R.; Teed, K.; Zavalij, L.; DeVita, J.; Tova, J.; Cotts, E.J.; Clum, J.A.; Erich, R.; Primavera, A.; Westby, G.; Coyle, R.J.; Wenger, G.M.; , "Solder metallization interdiffusion in microelectronic interconnects," *Components and Packaging Technologies, IEEE Transactions on* , vol.23, no.2, pp.383-387, Jun 2000 doi: 10.1109/6144.846778
6. Lee, C.C.; Jongsung Kim; "Fundamentals of fluxless soldering technology," *Advanced Packaging Materials: Processes, Properties and Interfaces, 2005. Proceedings. International Symposium on* , vol., no., pp. 33- 38, 16-18 March 2005 doi: 10.1109/ISAPM.2005.1432041
7. Massalski, B.; *Binary Alloy Phase Diagrams*. ASM International. 2nd Ed. Vol 2. Pg. 434
8. Holman, J.P., *Heat Transfer*. McGraw Hill, 9th Ed. Table A-2. "Property values for metals."
9. Sumitomo Bakelite North America RX® 790 Fiberglass Reinforced Phenolic Novolac
10. Scotch-Weld™ Epoxy Adhesives DP-469 Off-White, DP-420 Off-White Data Sheet, September, 1997, www.3m.com

This work performed under the auspices of the U.S. Department of Energy by Lawrence Livermore National Laboratory under Contract DE-AC52-07NA27344.